PAPER

A novel strategy to enhance ultraviolet light driven photocatalysis from graphene quantum dots infilled TiO$_2$ nanotube arrays†

Bipin Kumar Gupta,*[a] Garima Kedawat,[b] Yogyata Agrawal,[a] Pawan Kumar,[a] Jaya Dwivedi[a] and S. K. Dhawan[a]

Herein, a novel strategy has been proposed to fabricate graphene quantum dots (GQDs) infilled titanium dioxide (TiO$_2$) nanotube arrays (NTAs) hybrid structure for dye degradation of methylene blue (MB) under UV light (365 nm) irradiation. GQDs are infilled inside the TiO$_2$ NTAs (*via* anodic oxidation of a Ti sheet) through an impregnation method. Moreover, the morphology of the TiO$_2$ NTAs is well maintained after filling the GQDs inside, which is favorable for mass transfer. The peak intensity of photoluminescence (PL) spectra of the GQDs infilled TiO$_2$ NTAs catalyst is lower than that of annealed TiO$_2$ NTAs and a strong violet UV emission is obtained at 387 nm upon 252 nm deep UV excitation. The photocatalytic activities of the TiO$_2$ NTAs are evaluated in terms of the efficiencies of photo-decomposition and adsorption of MB in aqueous solution under UV light irradiation, after the impregnation of GQDs inside the TiO$_2$ NTAs. The highly-efficient photocatalytic activity is attributed to the broad absorption in the visible wavelength region, large photo-induced charge separation through the transfer of photo-generated electrons from the TiO$_2$ NTAs to GQDs, as well as the strong adsorption capacity of the GQDs to MB molecules. Thus, the GQDs infilled TiO$_2$ NTAs could be widely used as a photocatalyst for treating organic contaminants in the field of environmental protection.

1. Introduction

Photocatalysts, which accelerate chemical reactions upon light irradiation, have been paid considerable attention in environmental remediation and solar fuels production due to their fascinating properties, such as quantum confinement and enhanced reactivity.[1–3] Photocatalysts have a high potential for a wide range of industrial applications, including mineralization of organic pollutants, purification of disinfects in water and air, production of renewable fuels and organic synthesis.[1,3] The degradation of organic dyes using semiconductor photocatalyst materials is a promising resolution for wastewater purification.[4,5]

Titanium dioxide (TiO$_2$), which has a low cost, non-toxicity, high redox-ability and chemical stability, has been extensively studied as a very attractive photocatalyst semiconductor for energy saving and environmental protection due to its intriguing optical and electric properties.[6–8] However, due to its wide band gap of ~3.2 eV, it can be excited only by the ultraviolet radiation that occupies about 4% of solar light, thus

confining its applications in various fields.[9,10] Moreover, it also exhibits poor visible light absorption, low efficiency in light utilization and high recombination rate of photo-generated electron/hole pairs in comparison to the time taken for the chemical interaction of TiO$_2$ with adsorbed contaminants, which greatly retard its photocatalytic performance.[11,12] In order to utilize solar energy radiation, the development of catalyst materials, which reduce the recombination charge carrier time and harvest more photons in the visible light region of the solar spectrum, has become an active research area in the recent years. Thus, substantial efforts have been adopted to modify the structures and properties of TiO$_2$, such as the charge separation efficiency and enhancing its photoactivity in the visible range.[9,13]

In particular, vertically aligned photocatalyst TiO$_2$ three-dimensional (3D) nanotube arrays (NTAs) have been engrossing attention to improve the photocatalytic activity of TiO$_2$ because of their high orientation, tunable mesopore size, high internal surface area, convenient recycling and ion-changeable ability between interfaces.[5,14,15] In addition to this, the TiO$_2$ photocatalyst has also been extensively studied with novel heterostructure functional materials, such as narrow band-gap semiconductors, metal and non-metal elements and dye molecules to increase the efficiency and range of photon absorption.[16–18] Carbon based materials, such as graphene oxide, graphene sheets and graphene quantum dots anchored

[a]*CSIR – National Physical Laboratory, Dr K. S. Krishnan Road, New Delhi, 110012, India. E-mail: bipinbhu@yahoo.com; Fax: +91-11-45609310; Tel: +91-11-45609385*

[b]*Department of Physics, University of Rajasthan, Jaipur, 302055, India*

† Electronic supplementary information (ESI) available. See DOI: 10.1039/c4ra14039g

with the TiO_2 photocatalyst are highlighted as cost-effective UV driven photocatalysts in the visible region with enhanced activity due to their retarded charge recombination, increased reaction sites and expanded light absorption range properties.[19,20] These nanostructures concentrate organics near the photocatalyst surface, which could facilitate the effective photodegradation of pollutants under UV light.

Graphene quantum dots (GQDs) have a perfect sp^2-hybridized two-dimensional (2D) honeycomb carbon structure with better electron-transport, electron-accepting and stable photoluminescence properties.[21,22] These have emerged and ignited tremendous research interest due to their pronounced quantum confinement and edge effects. In particular, owing to their zero band gap, large surface area and high electron mobility, they also provide a direct path to the charge-transport of photo-generated charge carriers, which increases the lifetime of electron–hole pairs, arising through the incident of light irradiation on TiO_2 NTAs.[21,22] Thus, their photocatalyst performances for environmental remediation and energy conversion applications become greatly enhanced. However, to the best of our knowledge, there are few reports on the heterojunction between GQDs and TiO_2 nanotubes for photocatalytic applications.[16,19,22–24] Herein, we demonstrate a novel method to fabricate an efficient GQDs infilled TiO_2 NTAs photocatalyst. The highly oriented TiO_2 3D NTAs and GQDs were fabricated by the anodic oxidation of a Ti sheet and facile chemical synthesis method, respectively. GQDs were drop casted for impregnation into the inter-tubular voids of vertically aligned annealed TiO_2 3D NTAs. The microstructure (XRD, Raman and XPS) analysis confirmed the formation of the TiO_2 anatase phase, GQDs and covalent bonds, which occurred between Ti and C atoms through the filling of GQDs into the TiO_2 NTAs. Their photocatalyst activity was determined by the degradation of methylene blue (MB) as an organic pollutant molecule under UV light (365 nm) irradiation, which displayed a strong optical response under the visible-light range, efficient separation of photogenerated electron–hole pairs, as well as high adsorption capacity for MB. Moreover, the photocatalytic activity, stability and reusability of the novel GQDs/TiO_2 3D NTAs hybrid structure were substantially enhanced as compared to the pristine GQDs and TiO_2 NTAs. The structure and interfacial electronic interaction between TiO_2 and GQDs were also systematically investigated.

2.   Experimental

2.1   Materials

The titanium (Ti) sheet (99.8% purity, size ~0.5 mm × ~20 mm × ~15 mm) and carbon fibers were purchased from Sigma-Aldrich and Fibre Glast Development Corporation, respectively. Methylene blue (MB) was obtained commercially from Aldrich Chemical Co. Ammonium fluoride (NH_4F), ethylene glycol ($C_2H_6O_2$), sodium carbonate (Na_2CO_3) and all other reagents were of analytical (AR) grade and used as received without further purification. Double distilled water was used throughout the experiments.

2.2   Synthesis of vertically aligned TiO_2 3D NTAs

Vertical aligned TiO_2 3D NTAs were fabricated by the anodic oxidation of a 0.5 mm thick Ti sheet. Prior to anodization, the Ti sheet was ultrasonically cleaned in acetone and ethanol, respectively. A schematic representation of the experimental setup is shown in Fig. 1. The electrochemical anodization of the Ti sheet was carried out using the two-electrode configuration with the Ti sheet as the test electrode and a platinum sheet as the counter electrode. Both of the electrodes were immersed in the electrolytic solution, which was contained in a beaker and these were kept apart at a distance of 2 cm and Cu-wires were used for the connection through the parallel electrodes. The cleaned Ti sheet was anodized at 40 V for 4 hours (condition optimized experimentally) in an electrolyte solution, which was composed of 0.3 wt% NH_4F and 5.0 vol% deionized water in an ethylene glycol solution. The obtained amorphous NTAs samples were annealed at 500 °C for 2 hours to acquire the pure anatase phase of vertically aligned TiO_2 3D NTAs. The surface morphology of the annealed samples was analyzed by scanning electron microscopy, which revealed that after the anodization and annealing process, the large outer diameter of the tube was ~110 nm with a length 2000 nm.

2.3   Synthesis of graphene quantum dots

Carbon fibers (0.30 g) were added into a 3 : 1 mixture of concentrated H_2SO_4 (60 mL) and HNO_3 (20 mL). The solution was ultrasonicated (frequency; 25 kHz) for 2 hours and stirred for 24 hours at different temperatures of 80 °C, 100 °C and 120 °C, respectively. Then, the mixture was cooled and diluted with deionized (DI) water (800 mL) and the pH was adjusted to about 8 using Na_2CO_3. The final solution was further dialyzed in a dialysis bag (retained molecular weight: 2000 Da) for 3 days and then, the graphene quantum dots (GQDs) were obtained.[25] Furthermore, to characterize the GQDs, the film of GQDs was deposited on a quartz plate.
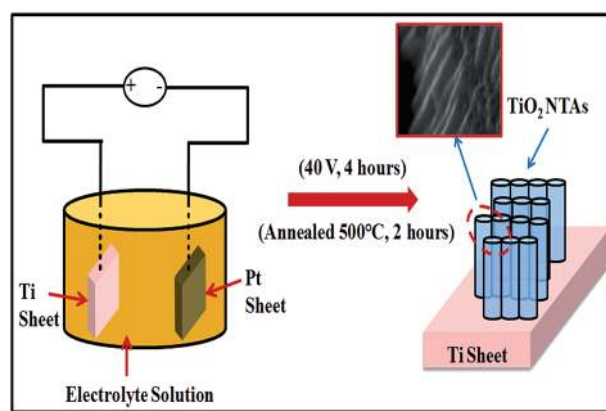

Fig. 1   Schematic representation of the experimental set-up of the electrochemical anodization process to obtain TiO_2 3D NTAs on a Ti sheet.

2.4 Synthesis of graphene quantum dots infilled TiO_2 3D NTAs

The as synthesized GQDs were ultrasonically dispersed into an ethanol solution *via* ultrasonication at a frequency of 25 kHz for 1 hour to form a homogeneous suspension with a concentration of 0.05 mg mL^{-1}. The resultant solution was drop casted on the mouth surface of the highly oriented TiO_2 3D NTAs (40 V, 4 hours, 500 °C) using a micro-syringe, as shown in Fig. 2. It is a highly-efficient technique to fill the GQDs into the TiO_2 nano-tubes, owing to its hydrophilic nature. Prior to infilling the GQDs in the TiO_2 nanotubes, the hydrophilic nature of the annealed TiO_2 3D NTAs was examined using contact angle measurements, which can be found in Fig. S1 (see ESI†). The contact angle between the TiO_2 3D nanotubes and a water droplet is about 0° and water is easily spread out on the TiO_2 nanotubes surface, which enables the quantum dots to make an easy entry into TiO_2 NTAs. Thus, this process provides the efficient entry of the GQDs through the hollow mouth of the TiO_2 nanotubes within few seconds. The contact angle experiment evidenced that it is possible to fill the water based GQDs efficiently into the TiO_2 NTAs, which can be clearly seen in Fig. 2. Several statistical runs have been performed to optimize the amount of drop, size and speed of the drop cast to avoid any kind of collapse of the TiO_2 nanotubes. After the drop cast process, once the infilling phenomenon is finished, the sample of the nanotube arrays was slowly washed with water multiple times to remove any kind of quantum dots stuck on the outer wall of the TiO_2 nanotubes. The infilled GQDs displayed chemical complexation with the internal walls of the TiO_2 nanotubes, which does not come out and does not even desorb when the GQDs infilled TiO_2 nanotube arrays samples are kept in aqueous solution or dispersed in aqueous solution as well as in any medium. The GQDs played a significant role in obtaining the enhanced photocatalyst activity of the TiO_2 NTAs.

2.5 Characterizations

The crystalline properties of the catalysts were evaluated by X-ray diffraction (XRD) measurements with a Rigaku Mini-flex
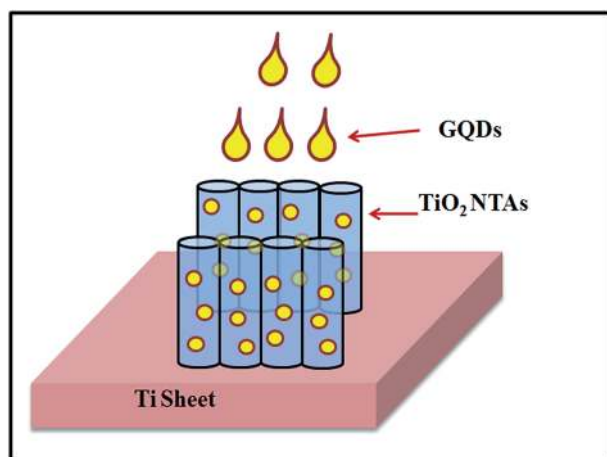

Fig. 2 The systematic process of GQDs infilled TiO_2 NTAs.

Diffractometer using Cu-Kα_1 radiation with a Ni filter (λ = 1.5406 Å at 30 kV and 15 mA). Prior to XRD measurements, the diffractometer was calibrated with silicon powder (d_{111} = 3.1353 Å).[26] Raman spectra were obtained using a Renishaw InVia Raman spectrometer, UK with an excitation source of 514.5 nm. The XPS analysis was performed in an ultra-high vacuum (UHV) chamber equipped with a hemispherical electron energy analyzer (Perkin Elmer, PHI1257) using a non-monochromatized Al Kα source (excitation energy of 1486.7 eV) with a base pressure of 4×10^{-10} torr at room temperature. The surface morphology, length and diameter of the TiO_2 NTAs were calculated by field emission scanning electron microscopy (FESEM, Model no. EVO-MA 10 VPSEM). The microstructural studies were performed using high-resolution transmission electron microscopy (HRTEM, Model no. Technai G20-twin, 200 kV with super twin lenses having a point and line resolution of 0.144 nm and 0.232 nm, respectively) equipped with energy dispersive X-ray analysis (EDAX) facilities. Photoluminescence (PL) spectra were obtained using a luminescence spectrometer (Edinburgh, FLSP – 920) with an EPL 375 nm picosecond pulsed diode laser as the source of excitation.

2.6 Photocatalytic degradation of MB

The relative photocatalytic activities of the GQDs infilled TiO_2 NTAs were evaluated by spectrophotometrically with an ATI Unicam UV spectrometer using a 1 cm quartz cuvette with a resolution of 2 nm. Prior to exposure to UV light, the GQDs infilled TiO_2 NTAs composite as photocatalyst was immersed into a MB solution (concentration 20 µM in water) for at least 45 min in a nitrogen atmosphere having dark medium until no further decrease of the absorption intensity of MB was observed. The optical absorption profiles were acquired at different exposure times to the UV light (365 nm, 6 W). Note that the solution was blanketed with a nitrogen atmosphere during the entire experimental procedure.

3. Results and discussion

The gross structures and phase analysis of the as-prepared samples were analyzed by XRD. Fig. 3 presents the XRD patterns of the annealed TiO_2 3D NTAs (Fig. 3a) and GQDs infilled TiO_2 3D NTAs (Fig. 3b). The quantitative analysis of Fig. 3a shows that all of the diffraction peaks are ascribed to the TiO_2 and Ti substrate. The typical diffraction peak (101) centred at 25.1° indicates the TiO_2 anatase phase (JCPDS no. 21-1272), which is formed after annealing at 500 °C for 2 hours. The peaks correspond to the (101), (103), (004), (112), (200), (105), (211), (213), (116) and (220) plane of the anatase phase with a tetragonal crystal structure with space group $I4_1/amd$ (141). The lattice parameters were calculated by the standard unit cell software with the help of obtained d-values and respective hkl planes, $a = b = (3.79632 \pm 0.0091)$ Å, $c = (9.5832 \pm 0.0097)$ Å for the annealed TiO_2 NTAs samples. Anatase TiO_2 exhibits a better performance due to the higher Fermi level and the lower recombination rate of its photo-generated electrons and holes than those of the rutile phase.[17] The average crystalline size for
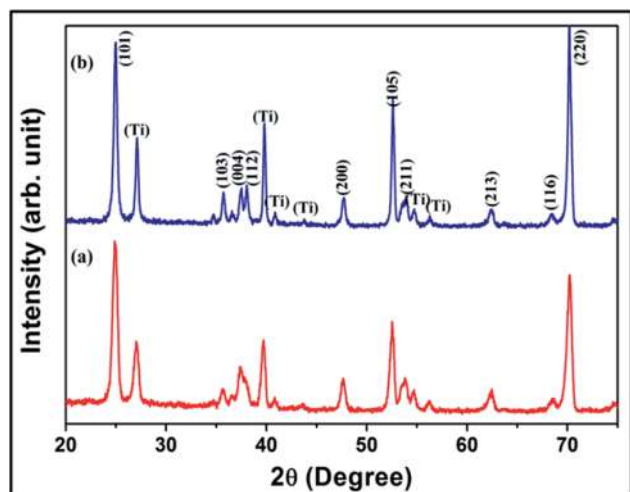
Fig. 3   The XRD patterns of (a) annealed TiO_2 3D NTAs and (b) GQDs infilled TiO_2 3D NTAs.
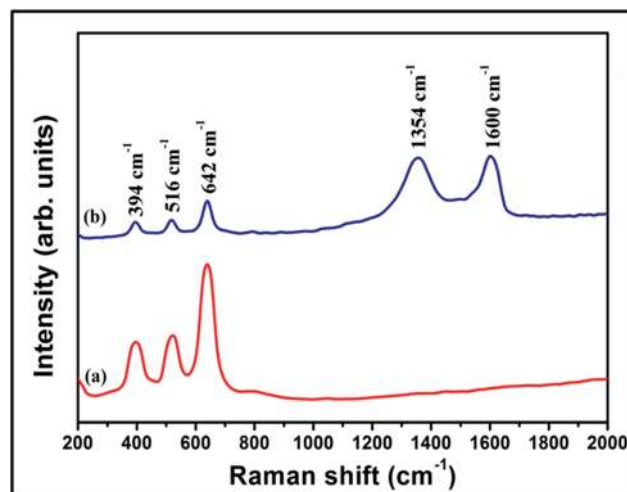

Fig. 4   Raman spectra of (a) annealed TiO_2 3D NTAs and (b) GQDs infilled TiO_2 3D NTAs.

the annealed TiO_2 3D NTAs samples is 121 nm with respect to the (101) plane, which is estimated using Scherrer's equation. It is noticed in Fig. 3b that diffraction patterns from the carbon species is not observed, which may result from the small amount and weak intensity of the GQDs and the main peak of graphene ($2\theta = 24°$) may have been shielded by the main peak of anatase TiO_2 at ($2\theta = 25.1°$).[20] There is no change in the phase of the TiO_2 NTAs, as in the annealed TiO_2 NTAs sample (Fig. 3a) and GQDs infilled annealed TiO_2 3D NTAs (Fig. 3b). These features indicate that the crystalline structure of the TiO_2 NTAs is not influenced by the filling of the GQDs into the TiO_2 3D NTAs. The XRD pattern of the GQDs is determined in Fig. S2a (see ESI†). The broad diffraction peak centered at $2\theta = 24.4°$ is attributed to the (002) plane of the carbon structure with a hexagonal phase (JCPDS no. 75-1621). The broad peak signifies the low crystallinity and small size of the GQDs, which have been verified with TEM measurements.

Raman spectroscopy was employed to confirm the formation of the TiO_2 anatase phase and the existence of GQDs in the inner walls of the TiO_2 NTAs. The Raman spectra of the annealed TiO_2 3D NTAs and GQDs infilled TiO_2 3D NTAs are shown in Fig. 4a and b, respectively. The Raman characteristic peaks for both samples at around 394, 516 and 642 cm^{-1} are obtained, which corresponds to the B_{1g}, $A_{1g} + B_{1g}$ and E_g modes of vibration of the anatase phase of TiO_2, respectively.[27] The observations are consistent with the XRD results. Two additional peaks at about 1354 and 1600 cm^{-1} for the graphene structure are also observed in the Raman spectrum of the GQDs infilled TiO_2 3D NTAs (Fig. 4b), which can be assigned to disordered sp^2 carbon (D-band) and well-ordered graphite (G-band), respectively.[25] The intensity ratio of the D to G band ($I_D/I_G = 0.846$) indicates a disorder in graphene, which originates from defects associated with grain boundaries, vacancies and amorphous carbons. The Raman spectrum of the GQDs is shown in Fig. S2b (see ESI†). This confirms the significant growth and incorporation of carbon on the internal surfaces of

TiO_2 nanotubes. The electronic interactions between graphene and TiO_2 components in the GQDs infilled TiO_2 3D NTAs were revealed by XPS measurements.

The GQDs infilled TiO_2 3D NTAs were employed for XPS analysis to detect the purity, bonding states and chemical composition of the TiO_2 nanotube and GQDs, and the XPS spectrum is shown in Fig. 5. It is a direct evidence for the TiO_2 band structure through the filling of GQDs. All the peak signals are endorsed to only titanium, oxygen and carbon elements, which show the high purity of the synthesized GQDs infilled TiO_2 3D NTAs. According to the XPS spectrum, the characteristic deconvolution peaks of the C1s, O1s and Ti(2p) core levels of the GQDs infilled TiO_2 3D NTAs are given in Fig. S3 (see ESI†). The graphene peak (Fig. S3a†) is assigned with the binding energy of the C1s electrons of sp^2 hybridized carbon at around 291 eV. The $Ti2p_{1/2}$ and $Ti2p_{3/2}$ electrons are attributed to the 463.9 eV and 458.24 eV binding energies for titanium
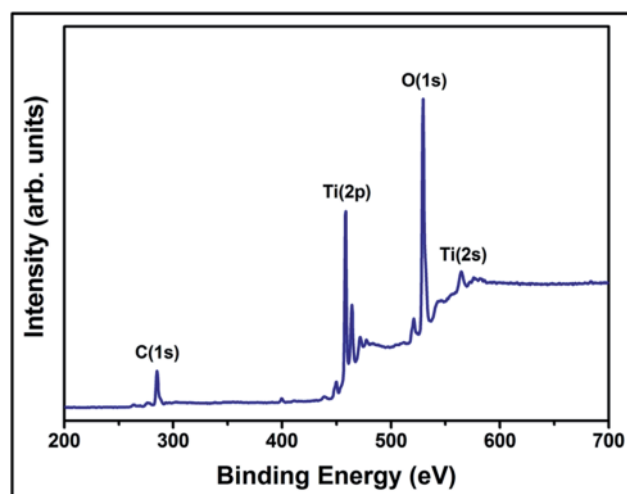

Fig. 5   XPS spectrum of GQDs infilled TiO_2 3D NTAs.

(Fig. S3b†), respectively and the O1s electron is obtained at the 529.5 eV binding energy for oxygen (Fig. S3c†) in the C1s infilled TiO_2 3D NTAs structure. The characteristic deconvolution peaks (filled area) of the C1s is given in Fig. S3a.†

The typical XPS peaks at 292.2, 293.1, and 295.2 eV appeared, which can be assigned to the presence of the C–C, C–O, and C=O functional groups, respectively. This intimate the electronic interactions between the carbon and TiO_2 nanotube in the GQDs infilled TiO_2 3D NTAs for the unique interfacial charge transfer under photo-irradiation process. For the morphological analysis, scanning electron microscopy (SEM) and transmission electron microscopy (TEM) were used to characterize the GQDs infilled TiO_2 3D NTAs structure. Fig. 6a–d represents the top and lateral views of the SEM images of the high density, vertically aligned, annealed TiO_2 3D NTAs formed on the Ti substrate with an average outer diameter of ∼110 nm and maximum length of ∼2000 nm. The alignment of sample was not disturbed after annealing and it consists of uniform open nanotubes of TiO_2 with good crystallinity.

To obtain the morphology, crystallite size and composition of the TiO_2 3D NTAs and GQDs infilled TiO_2 3D NTAs, the TEM images and EDX spectrum are analyzed in Fig. 7. The TEM image of an isolated annealed TiO_2 nanotube with an outer diameter of ∼110 nm is depicted in Fig. 7a and the inset shows the HRTEM image of the TiO_2 3D NTAs with high quality lattice fringes without distortion. It clearly demonstrates the crystal quality of TiO_2 nanotubes, which is consistent with the XRD results. The precise observation of the HRTEM image indicates that the estimated interplanar spacing of the adjacent lattice fringes, as highlighted by black lines, is estimated to be ∼0.35

nm which corresponds to the (101) plane of TiO_2 anatase phase. The TEM image of the GQDs is shown in Fig. 7b. The GQDs are found to exhibit a narrow size distribution with an average crystallite size of ∼8–12 nm. The HRTEM image of the GQDs with ∼0.40 nm interplanar spacing of adjoining lattice fringes corresponding to the (002) plane of the GQDs is shown in the inset of Fig. 7b. The TEM image of the GQDs infilled TiO_2 3D NTAs is given in Fig. 7c, where the yellow circle represents the GQD particle. The graphene is well established in binding to the TiO_2 nanotube through covalent bonding or complexation without aggregation effects. The strong interaction between the GQDs and TiO_2 would allow the transfer of electrons from TiO_2 to the GQDs during the photo-irradiation process, which could significantly increase the separation of photo-induced charges and lead to an improved photocatalytic activity in the degradation of organic pollutants. Furthermore, the evidence of quality as well as elemental composition of the TiO_2 nanotubes and GQDs were evaluated by the EDAX analysis. The spot EDAX measurement was performed with a reduced beam spot size and low accelerating potential to enhance signal to noise ratio. The EDAX spectrum of the GQDs infilled TiO_2 3D NTAs is also shown in Fig. 7d. The EDAX analysis indicates the presence of titanium, oxygen, fluorine, and carbon elements in the GQDs infilled TiO_2 3D NTAs composite structure. The carbon content is presented in a relatively lower intensity as compared to the higher intensity of the titanium and oxygen content. The presence of the fluorine element is due to the electrolyte solution. Further, a typical HRTEM image was taken to evidence the interface between the GQDs and TiO_2, as shown in inset of Fig. 7d. The yellow mark line clearly reveals the separate lattice
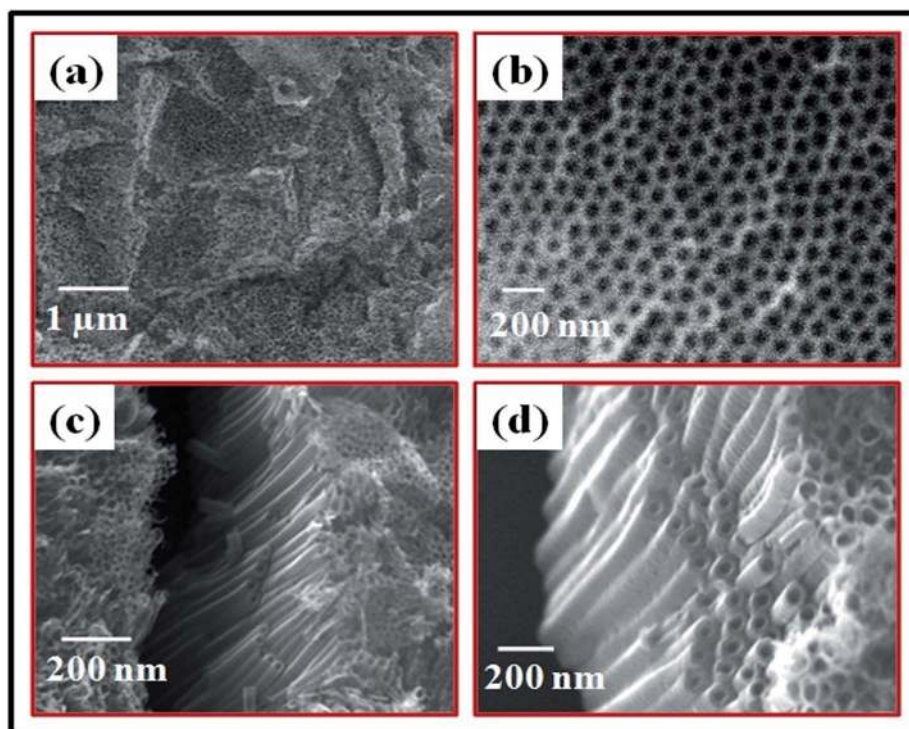

Fig. 6 SEM images; (a) top view, (b) magnified view of (a), (c) lateral view and (d) magnified view of (c) of annealed TiO_2 3D NTAs.
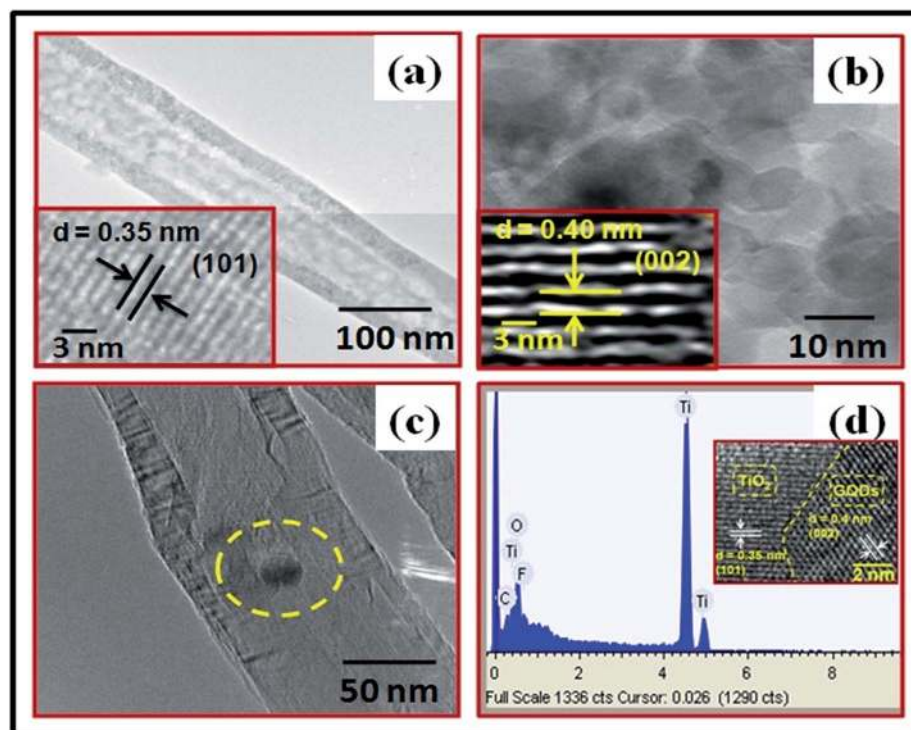
Fig. 7 (a) TEM image of an isolated annealed TiO_2 nanotube; inset shows the HRTEM image of (a), (b) TEM image of GQDs; inset shows the HRTEM image of (b), (c) TEM image of GQDs infilled isolated TiO_2 nanotube; yellow circle represents the GQD particle and (d) EDAX spectrum of GQDs infilled TiO_2 3D NTAs; inset shows the HRTEM image of GQDs infilled TiO_2 NTAs where yellow mark line clearly reveals the separate lattice of the GQDs and TiO_2.

of the GQDs and TiO_2 with their estimated d-spacing. The GQDs are well established in binding to TiO_2 nanotubes through covalent bonding or complexation without aggregation effects.

Photoluminescence (PL) is an essential direct optical probe to investigate the efficiency of charge carrier trapping and understand the rate of e^-/h^+ pairs in semiconductor particles. The PL emission spectra of the annealed TiO_2 NTAs and GQDs infilled TiO_2 3D NTAs at the 252 nm excitation wavelength is exhibited in Fig. 8 and the inset shows the CIE (chromaticity diagram) color coordinates of the annealed TiO_2 3D NTAs, which is obtained from the emission spectrum of the annealed TiO_2 nanotube using chromaticity diagram, $x = 0.2243$ and $y = 0.1808$. The optical image of the sample chamber of the PL spectrometer is given in Fig. S4 (see ESI†), where the annealed TiO_2 3D NTAs on the Ti sheet were loaded. The annealed TiO_2 3D NTAs sample is shown in Fig. S4a.† The annealed TiO_2 3D NTAs sample was placed in the spectrometer chamber to optimize the position of the TiO_2 3D NTAs. The sample exhibits a strong violet UV emission under deep UV light at the 252 nm excitation wavelength, which is shown in Fig. S4b.† The strong ultraviolet emission near the visible region of 387 nm (~3.2 eV) was observed, as shown in Fig. 8; the excitation wavelength is 252 nm. The PL results reveal that the intensity of the annealed TiO_2 is higher than the GQDs infilled TiO_2 3D NTAs, which were expected because the annealing at 500 °C, which is a higher temperature, introduced more defects and oxygen vacancies in the TiO_2 NTAs and strong PL occurs. The reduction of the PL

emission intensity suggests that the GQDs in the hybrid structure can restrain the recombination of electrons and holes and promotes the separation of electron–hole pairs and extends the life of electrons. The PL spectra with a peak at 387 nm (~3.2 eV)
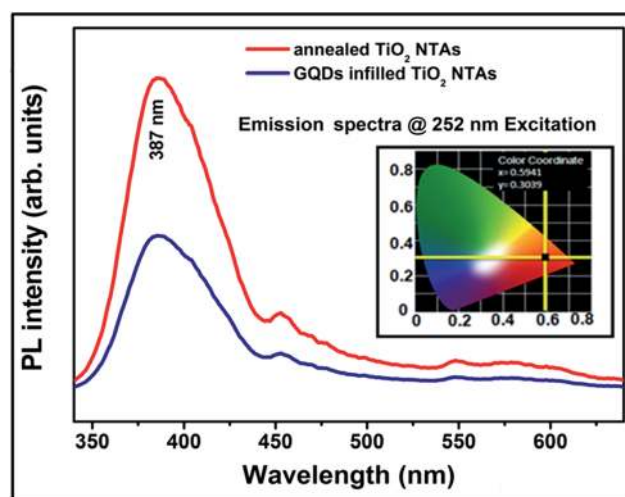

Fig. 8 The PL emission spectra of the annealed TiO_2 NTAs and GQDs infilled TiO_2 3D NTAs at the 252 nm excitation wavelength; inset exhibits the CIE (chromaticity diagram) color coordinates of the annealed TiO_2 3D NTAs, which is obtained from the emission spectra of the annealed TiO_2 nanotube using the chromaticity diagram, $x = 0.2243$ and $y = 0.1808$.

correspond to the direct recombination between electrons in the conduction band and holes in the valence band. The other two broad peaks at 454 nm (~2.73 eV) and 548 nm (~2.26 eV) within the visible wavelength region corresponds to defects induced photoluminescence either *via* oxygen defects and impurities or due to the surface states induced at the annealing temperature. The estimated band gap from the annealed TiO_2 3D NTAs PL spectrum is ~3.2 eV. It very closely matches with the estimated band gap from other spectroscopic techniques and also confirms the anatase phase of the annealed TiO_2 nanotubes. The PL spectrum of the GQDs is shown in Fig. S2c (see ESI†) and the inset shows a strong blue emission at the 320 nm excitation wavelength. A broad peak at 430 nm strong blue emission is observed at the 320 nm excitation wavelength.

The optical absorption spectra of the annealed TiO_2 3D NTAs and GQDs infilled TiO_2 3D NTAs are shown in Fig. S5 (see ESI†). The samples were dispersed in water and sonicated for 10 min in an ultra-sonication bath. Further, the solution was put in a quartz cuvette for the UV-visible absorption analysis, which reveals the absorption peak at ~387 nm shown in Fig. S5a.† It can be noticed that the intensity of the absorption spectra is higher in case of the GQDs infilled TiO_2 3D NTAs sample. The band gap of the annealed sample is estimated using the Tauc equation. It is found to be ~3.2 eV, which is expected for the TiO_2 anatase phase. The optical absorption spectra of the annealed TiO_2 3D NTAs and GQDs infilled TiO_2 3D NTAs samples are also taken with a visible light source (mercury lamp) in the range of 400–700 nm, as shown in Fig. S5b.† No significant change was observed in the presence of a visible light source as compared to the UV-vis absorption spectra. Thus, most of the photocatalyst phenomenon is driven under UV light. The photocatalyst activity enhancement of the GQD infilled TiO_2 3D NTAs was examined using the reduction of MB in the present investigation. The UV-vis absorption spectra of the MB solution after exposure to UV photo-irradiation for different periods of time in the presence of the GQD infilled TiO_2 3D NTAs is shown in Fig. 9. The absorption of MB is very strong in the visible range with two well-defined absorption peaks at 612 and 663 nm and the reduced form is colorless. After the illumination of UV light, electrons are excited from the TiO_2 valence band to the conduction band. The photo-generated electrons may then be exploited for the reduction of MB. As oxygen is an effective electron scavenger and it is enhanced by introducing GQDs into the TiO_2 nanotubes, it is important to notice that the reaction media was protected with an inert atmosphere of nitrogen. The absorption features diminish rather quickly upon UV photo-irradiation, suggesting the effective photocatalytic activity of the GQD infilled TiO_2 in the reduction of MB due to the additional surface provided by the GQD as well as additional UV light absorbed through the GQDs surface. The variation of the intensity of the absorption peak at 665 nm with UV exposure time is presented in the inset of Fig. 9. It is clear that the absorption peak decreases with respect to time. Thus, the introduction of GQDs into the TiO_2 3D NTAs could expand the light absorption range for broad range of visible light.
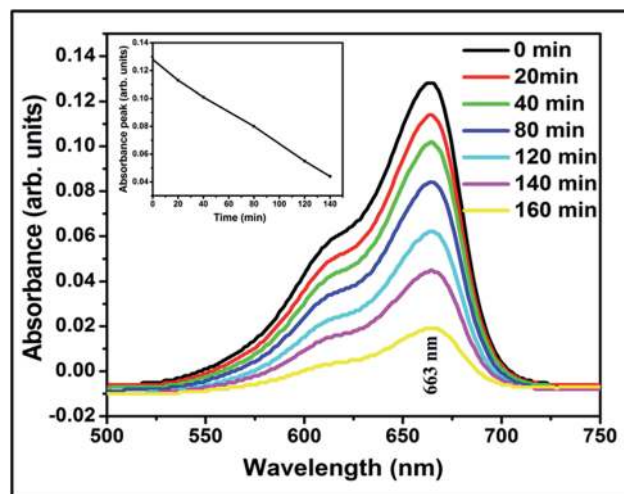

Fig. 9 (a) UV-vis absorption spectra of a MB solution (25 μM in water) after being exposed to UV photo-irradiation for different periods of time in the presence of GQD infilled TiO_2 3D NTAs and inset shows the spectrum of variation of intensity of the absorption peak at 663 nm with UV exposure time for GQD infilled TiO_2 3D NTAs.

The photocatalytic kinetic activities of the GQDs infilled TiO_2 NTAs were evaluated by the photocatalytic degradation of MB in water under UV irradiation and these were compared with the photocatalytic activity of pristine methylene blue, commercial TiO_2 (purchase from Sigma Aldrich, 99.99 purity, size ~50 nm), as-synthesized TiO_2 nanotubes and annealed TiO_2 nanotubes, as shown in Fig. 10a. It can be seen that the additional surface area and optical properties of the GQDs and the crystallinity of annealed TiO_2 have a strong influence on the photocatalytic activities. The C/C_0 ratio of the GQDs infilled TiO_2 nanotubes, annealed TiO_2 nanotubes, as synthesized TiO_2 nanotubes, commercial TiO_2 nanostructures and MB are 0.009, 0.12, 0.39, 0.52 and 0.70, respectively after 180 min irradiation time. In the absence of GQDs, electrons are excited from the valence band (VB) to the conduction band (CB) of TiO_2 and then holes are created in the valence band. Most of these charges recombine and only a small fraction participates in photocatalytic reactions, which decrease the photo-efficiency. Further, after filling the GQDs in the TiO_2 NTAs, the degradation rate was faster than the other samples under the same irradiation time and this sample exhibited superior photocatalytic activity for the degradation of MB. About ~99.8% of MB was decomposed with GQDs infilled TiO_2 annealed samples in 180 min time duration, which may arise from the narrow band gap, reduced charge carriers recombination rate, stabilization and fast electron transport through the GQDs.

Besides its high activity, the stability of the GQDs infilled TiO_2 NTAs sample was also investigated. We examined the stability of the GQDs infilled TiO_2 NTAs by repeating the photocatalytic degradation of MB for 10 cycles and the calculated data are given in Fig. 10b. It can be seen that the GQDs infilled TiO_2 NTAs sustained the high and stable degradation efficiency of 95.5% after the 10th recycle. The excellent cycling stability is consistent with the nearly unchanged absorption in the visible
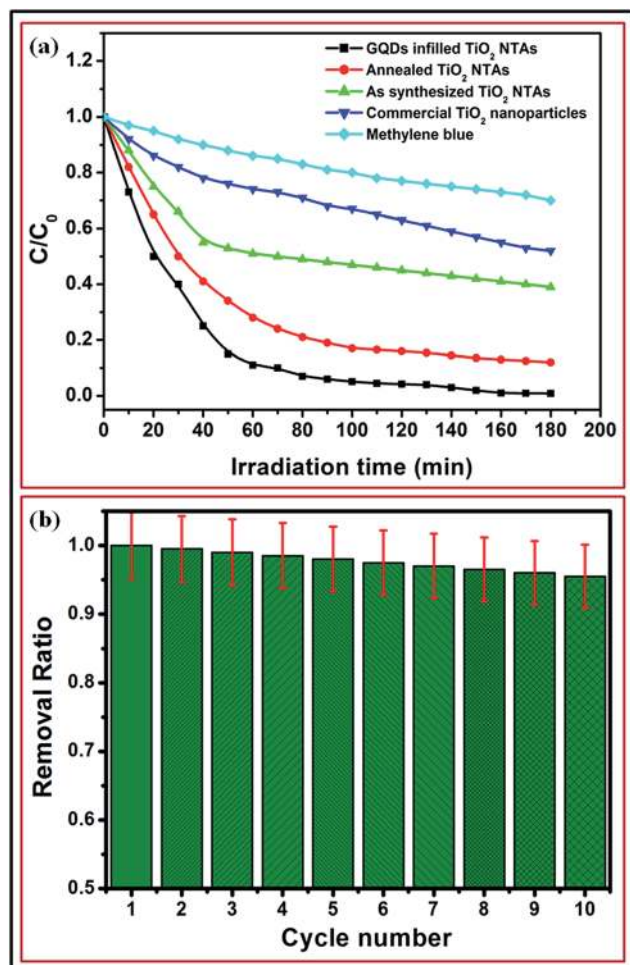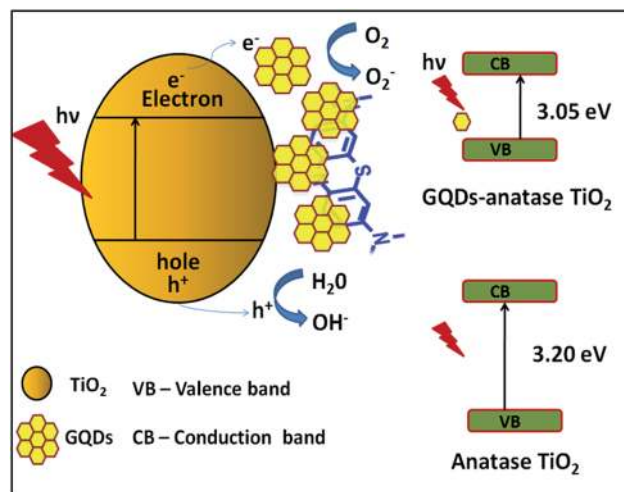
Fig. 10 (a) Comparative studies on photocatalytic activity *versus* UV irradiation time for pristine methylene blue, commercial TiO_2 (size ~50 nm), as synthesized TiO_2 nanotubes, annealed TiO_2 nanotubes and GQD infilled TiO_2 NTAs and (b) cycle stability data of the GQD infilled TiO_2 NTAs.

Scheme 1 Schematic illustration of the methylene blue photo-degradation process for GQD infilled TiO_2 nanotube arrays hybrid structure under UV light ($\lambda \sim 365$ nm) irradiation.

and large aromatic domains of the GQDs creates a high affinity, good electrical conductivity and adsorptivity of MB. Moreover, the large specific surface area of the GQDs also increases the adsorption of the MB molecules. Therefore, in the photo-degradation of MB, the GQDs play an important role to enhance the photocatalytic activity over the pristine TiO_2 NTAs.

4. Conclusions

A facile method has been demonstrated for the fabrication of GQDs (~8–12 nm) infilled TiO_2 NTAs (~110 nm in diameter) by the impregnation of GQDs into TiO_2 nanotubes 3D arrays. The TiO_2 crystallographic structure remained almost identical for all the composites, and the TiO_2 anatase phase was confirmed from both XRD and Raman spectroscopy. Microscopy and spectroscopic studies revealed the incorporation of GQDs into the TiO_2 NTAs and the optimal assembly and interfacial coupling between the GQDs and TiO_2 nanotubes, respectively. The activity of the GQDs infilled TiO_2 NTA hybrid structure expanded the light absorption and enhanced the photocatalytic decomposition of MB molecules in aqueous solution under UV light irradiation. This might be attributed to the large surface area of GDQs and narrow band gap of TiO_2 in the composite, which would allow greater adsorption of visible light, efficient electron transfer from TiO_2 to GQDs, prolonged recombination rate of charge carriers and oxidation of adsorbed molecules. Thus, it is a scalable and cost-effective approach for the fabrication of GQDs infilled TiO_2 NTAs as an efficient multifunctional photocatalyst for the degradation of hazardous compounds in waste water.

Acknowledgements

region. This high cycling stability and reusability of the GQDs infilled TiO_2 nanotubes arrays is ascribed to a promising candidate for photocatalytic applications. After the stability test, we again examined the micro structural morphology of the GQDs infilled TiO_2 nanotubes arrays by TEM microscopy, which is shown in Fig. S6 (see ESI†). The TEM image shows that the GQDs remains in the TiO_2 nanotube and does not have any effect on the GQDs after the 10th cyclability test. The surface roughness of the TiO_2 nanotube slightly increases. A schematic illustration of the methylene blue photo-degradation process for the GQDs infilled TiO_2 nanotube array hybrid structure under UV light irradiation is shown in Scheme 1. Upon UV light irradiation, TiO_2 yields electron–holes and electrons are scavenged by oxygen and GQDs to generate "OH^{-1}" radicals and "O^{2-} or H^+" intermediate species by reacting with absorbed H_2O molecules for the photo-decomposition of MB. Thus, the photogenerated charges are separated efficiently and transferred from the TiO_2 conduction band to the GQD for radical generation. The strong π–π stacking interaction between the MB molecules

References

1 A. Fujishima and K. Honda, *Nature*, 1972, **238**, 37–38.

2 J. Xing, W. Fang, H. Zhao and H. Yang, *Chem.–Asian J.*, 2012, **7**, 642–657.

3 N. Wu and M. Lee, *Int. J. Hydrogen Energy*, 2004, **29**, 1601–1605.

4 M. L. Curri, R. Comparelli, P. D. Cozzoli, G. Mascolo and A. Agostiano, *Mater. Sci. Eng., C*, 2003, **23**, 285–289.

5 X. Kang and S. Chen, *J. Mater. Sci.*, 2010, **45**, 2696–2702.

6 J. Zhang, Q. Xu, Z. Feng, M. Li and C. Li, *Angew. Chem., Int. Ed.*, 2008, **47**, 1766–1769.

7 M. J. Uddin, M. M. Alam, M. A. Islam, S. R. Snigda, S. Das, M. M. Rahman, M. N. Uddin, C. A. Morris, R. D. Gonzalez, U. Diebold, T. J. Dickens and O. I. Okoli, *Int. Nano Lett.*, 2013, **3**, 16–26.

8 M. Ni, K. H. Leung, D. Y. C. Leung and K. Sumathy, *Renewable Sustainable Energy Rev.*, 2007, **11**, 401–425.

9 X. Chen and S. S. Mao, *Chem. Rev.*, 2007, **107**, 2891–2895.

10 G. Liu, L. Wang, H. G. Yang, H. M. Cheng and G. Q. Lu, *J. Mater. Chem.*, 2010, **20**, 831–843.

11 M. A. Fox and M. T. Dulay, *Chem. Rev.*, 1993, **93**, 341–357.

12 T. Wu, G. Liu, J. Zhao, H. Hidaka and N. Serpone, *J. Phys. Chem. B*, 1999, **103**, 4862–4867.

13 T. Kako, N. Umezawa, K. Xie and J. Ye, *J. Mater. Sci.*, 2013, **48**, 108–114.

14 J. Macak, M. Zlamal, J. Krysa and P. Schmuki, *Small*, 2007, **3**, 300–304.

15 P. Roy, S. Berger and P. Schmuki, *Angew. Chem., Int. Ed.*, 2011, **50**, 2904–2939.

16 Y. Chen, Y. Tang, S. Luo, C. Liu and Y. Li, *J. Alloys Compd.*, 2013, **578**, 242–248.

17 C. H. Kim, B. H. Kim and K. S. Yang, *Carbon*, 2012, **50**, 2472–2481.

18 M. Nolan, *Chem. Commun.*, 2011, **47**, 8617–8619.

19 Y. Yu, J. Ren and M. Meng, *Int. J. Hydrogen Energy*, 2013, **38**, 12266–12272.

20 P. Song, X. Zhang, M. Sun, X. Cui and Y. Lin, *Nanoscale*, 2012, **4**, 1800–1804.

21 S. Zhu, J. Zhang, X. Liu, B. Li, X. Wang, S. Tang, Q. Meng, Y. Li, C. Shi, R. Hu and B. Yang, *RSC Adv.*, 2012, **2**, 2717–2720.

22 S. Zhuo, M. Shao and S. T. Lee, *ACS Nano*, 2012, **6**, 1059–1064.

23 J. Shen, Y. Zhu, X. Yang and C. Li, *Chem. Commun.*, 2012, **48**, 3686–3699.

24 D. Pan, C. Xi, Z. Li, L. Wang, Z. Chen, B. Luc and M. Wu, *J. Mater. Chem. A*, 2013, **1**, 3551–3555.

25 J. Peng, W. Gao, B. K. Gupta, Z. Liu, R. Romero-Aburto, L. Ge, L. Song, L. B. Alemany, X. Zhan, G. Gao, S. Antony Vithayathil, B. A. Kaipparettu, A. A. Marti, T. Hayashi, J. J. Zhu and P. M. Ajayan, *Nano Lett.*, 2012, **12**, 844–849.

26 G. Kedawat, S. Srivastava, V. K. Jain, P. Kumar, V. Kataria, Y. Agrawal, B. K. Gupta and Y. K. Vijay, *ACS Appl. Mater. Interfaces*, 2013, **5**, 4872–4877.

27 T. Ohsaka, F. Izumi and Y. Fujiki, *J. Raman Spectrosc.*, 1978, **7**, 321–324.